Electrochemical p-Doping of $CsPbBr_3$ Perovskite Nanocrystals

Mulder, Jence T.; Du Fossé, Indy; Alimoradi Jazi, Maryam; Manna, Liberato; Houtepen, Arjan J.

DOI
10.1021/acsenergylett.1c00970

Publication date
2021

Document Version
Final published version

Published in
ACS Energy Letters

ACS Energy LETTERS

http://pubs.acs.org/journal/aelccp

Electrochemical p-Doping of $CsPbBr_3$ Perovskite Nanocrystals

Jence T. Mulder, Indy du Fossé, Maryam Alimoradi Jazi, Liberato Manna, and Arjan J. Houtepen*

Cite This: *ACS Energy Lett.* 2021, 6, 2519–2525

Read Online

ACCESS | Metrics & More | Article Recommendations | Supporting Information

ABSTRACT: **Lead halide perovskite nanocrystals have drawn attention as active light-absorbing or -emitting materials for opto-electronic applications due to their facile synthesis, intrinsic defect tolerance, and color-pure emission ranging over the entire visible spectrum. To optimize their application in, e.g., solar cells and light-emitting diodes, it is desirable to gain control over electronic doping of these materials. However, predominantly due to the intrinsic instability of perovskites, successful electronic doping has remained elusive. Using spectro-electrochemistry and electrochemical transistor measurements, we demonstrate here that $CsPbBr_3$ nanocrystals can be successfully and reversibly p-doped via electrochemical hole injection. From an applied potential of ∼0.9 V vs NHE, the emission quenches, the band edge absorbance bleaches, and the electronic conductivity quickly increases, demonstrating the successful injection of holes into the valence band of the $CsPbBr_3$ nanocrystals.**

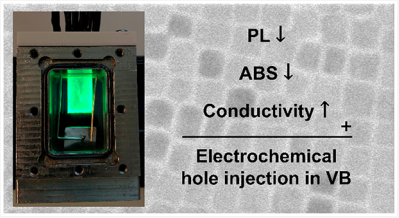

Since the discovery of lead halide perovskite nanocrystals (NCs) in 2014,[1] these materials have been investigated as candidates for downconversion phosphors,[2−4] absorber layers in solar cells,[5−7] and emitting layers in light-emitting diodes (LEDs).[8−14] Important advantages of perovskite NCs are their facile synthesis[15−18] and their intrinsic defect tolerance.[19−24] As with all semiconductor materials, controlling the carrier density via electronic doping is key to tailoring the optoelectronic properties and implementation in devices.[25,26] This could allow, for instance, rational design of *pn* junction LEDs[27−29] or low threshold lasers.[30]

However, electronic doping is often challenging, and effects like doping compensation or self-purification can prevent control over the carrier concentration.[31,32] Especially for perovskites, which are complex compound semiconductors with a low stability, changing the Fermi level via doping could have many effects, including the decomposition of the material itself. As a result, electronic doping of perovskites, and perovskite NCs, has remained a challenge.[33] Some works have reported the use of, e.g., Ag as a substitutional dopant,[34] but this resulted in only mild p-doping (Fermi level still 0.6 eV above the VB edge). In addition, incorporation of impurities generally has detrimental effects on the structural and electronic properties of the NCs.[26] Use of external dopants, such as charge-transfer complexes, has the advantage of not introducing impurities into the crystal.[35,36] However, this has also resulted in only mild p-doping, with an increase of p-type conductivity of roughly a factor of 2 compared to undoped films.[35]

A much higher extent of charging with external dopants is possible for semiconductor films that are permeable to electrolyte ions by means of electrochemical electron or hole injection. The electrolyte ions act as external dopants, without compromising the structure of the semiconductor material, and without introducing dopant energy levels in the bandgap, as has been demonstrated for, e.g., quantum dots,[37−41] conducting polymers,[42,43] and transition metal dichalcogenides.[44,45] Further advantages of electrochemical doping are that the Fermi level can be controlled by the applied potential and that charge injection is reversible. Electrochemical doping of perovskite NCs, however, has been challenging because the NCs can readily undergo electrochemical decomposition reactions. For instance, the application of negative potentials easily results in cathodic decomposition via lead ion reduction, an effect that we confirm here.[46] As a result, previous reports on the electrochemistry of perovskite NCs[47] and perovskite thin films[46] have not yet proven successful n- or p-doping.

Here we report reversible electrochemical p-doping of $CsPbBr_3$ perovskite NCs. First, we use spectro-electrochemistry to investigate the optical and electronic properties of $CsPbBr_3$ perovskite NCs as a function of electrochemical potential. While potentials more negative than −0.6 V vs NHE

Received: May 11, 2021
Accepted: June 15, 2021
Published: June 17, 2021

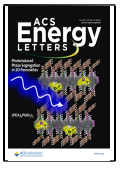

https://doi.org/10.1021/acsenergylett.1c00970
ACS Energy Lett. 2021, 6, 2519–2525

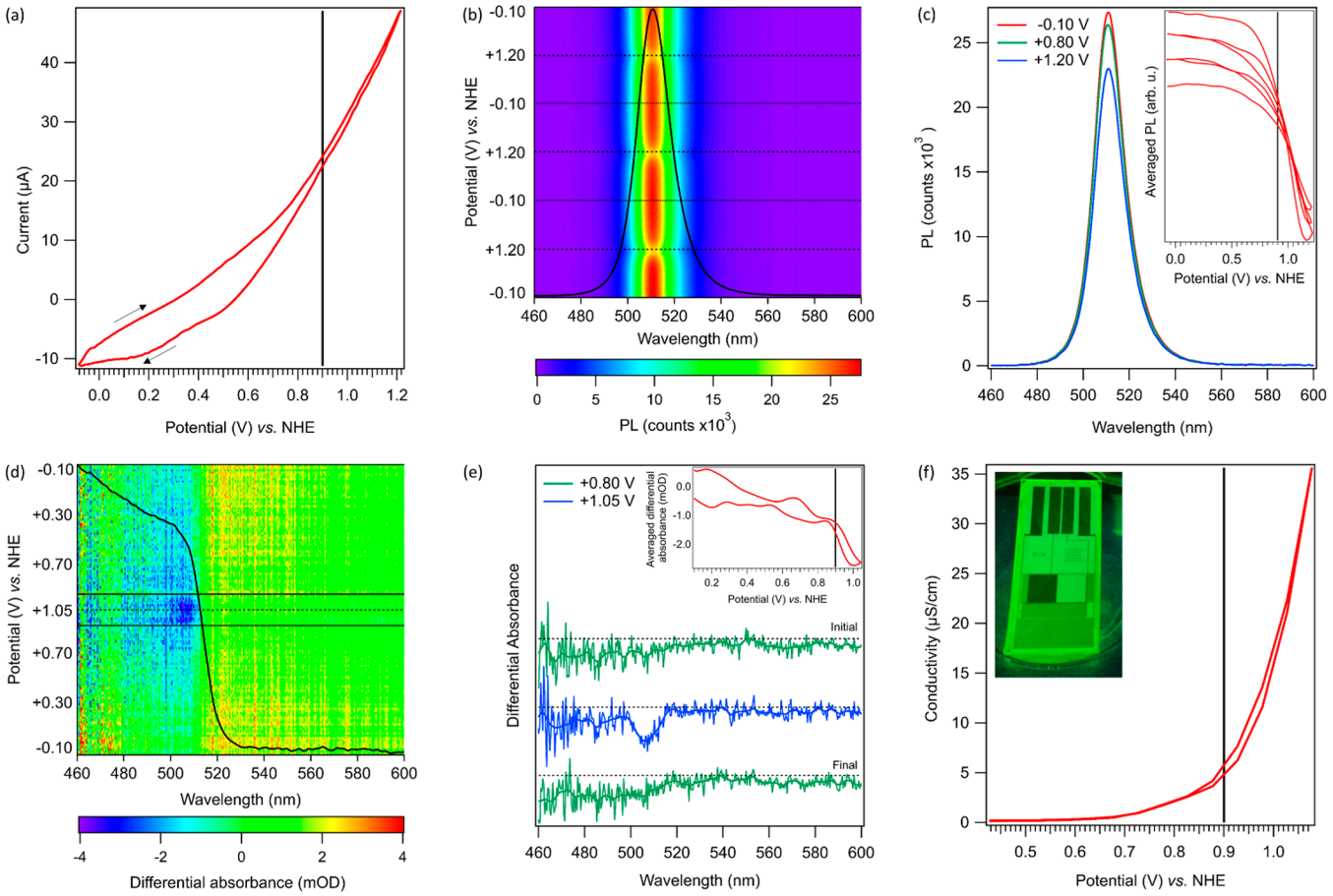

Figure 1. (a) CV of a $CsPbBr_3$ NC electrode (scan speed 20 mV/s). The estimated VB edge position is marked by the black line. (b) PL of a NC electrode as a function of the applied potential during three CV scans ranging from −0.10 to +1.20 V. Hole injection into the VB edge of the NCs, starting at +0.9 V, quenches the PL, which largely recovers when the applied potential is lowered to below +0.9 V. (c) PL spectra of the NC electrode shown in (b) at −0.10, +0.80, and +1.20 V during the first scan. Inset: the averaged PL between 500 and 520 nm as a function of applied potential, featuring a sharp decrease in intensity once the VB edge is reached, followed by nearly full recovery. (d) Differential absorbance of a NC electrode as a function of the applied potential, ranging from −0.10 to +1.05 V. The initial absorption spectrum is plotted in black. (e) Differential absorbance spectra at +0.80 and +1.05 V, characterized by a reversible bleach of the band edge absorption feature. Inset: differential absorbance at the band edge (averaged between 500 and 510 nm). (f) The conductivity of a NC film over the applied potential range obtained from a source−drain potential of 50 mV between the two electrodes. Inset: the NC electrode that was used for the conductivity measurements.

(N.B.: All potentials reported in this work are referenced vs NHE.) result in irreversible changes in the optical properties due to Pb^{2+} reduction before electrons can be injected into the conduction band (CB), the changes at positive potentials are much more controllable and reversible. At potentials more positive than +0.9 V, we observe reversible bleaching of the band edge absorption and quenching of the photoluminescence (PL). Electrochemical transistor measurements indicate a concomitant reversible increase in electronic conductivity, indicating that we can reversibly p-dope the NCs by hole injection into the valence band (VB). In accordance with these experimental results, density functional theory (DFT) calculations demonstrate that injected holes remain delocalized in the VB, whereas electron injection leads to charge localization on Pb^{2+}, confirming the much higher stability of $CsPbBr_3$ NCs at positive than at negative potentials.

The $CsPbBr_3$ NCs used in this work were synthesized by the method of Imran et al.[48] (see Supporting Information (SI), section SI-1), which employs benzoyl bromide as the halide source. This synthesis method was chosen over the method of Protesescu et al.[49] (used by previous work[46,47]) which uses lead bromide as the halide source, as the NCs synthesized with benzoyl bromide are not halide poor. The halide-rich conditions result in a larger fraction of oleylammonium ions, bound to bromide ions on the NC surface, which leads to a high photoluminescence quantum yield and improved resistance to washing.[48] The NCs have an average size of 10 nm, a band edge absorption at ∼505 nm, and a PL maximum at 511 nm (see SI, Figures S-1 and S-2). NC films were drop-cast on ITO substrates or interdigitated gold electrodes, with 1,8-octanedithiol as cross-linking ligands (see SI-1 for details). As shown in Figure S-1, this resulted in highly luminescent NC films, and the fabrication of the films did not affect the absorption and emission spectra or the size or shape of the NCs. Subsequently, the absorption and PL of the NC electrodes were measured while varying the potential via cyclic voltammetry (CV, see SI-1 for details). The CV started at the open-circuit potential (V_{oc}) of −0.1 V vs NHE (from here on, the reference "vs NHE" will be omitted) and was first scanned to more positive potentials (scan rate 20 mV/s). As shown in Figure 1a, the CV features a significant irreversible anodic current at potentials >0.6 V, probably due to

https://doi.org/10.1021/acsenergylett.1c00970
ACS Energy Lett. 2021, 6, 2519−2525

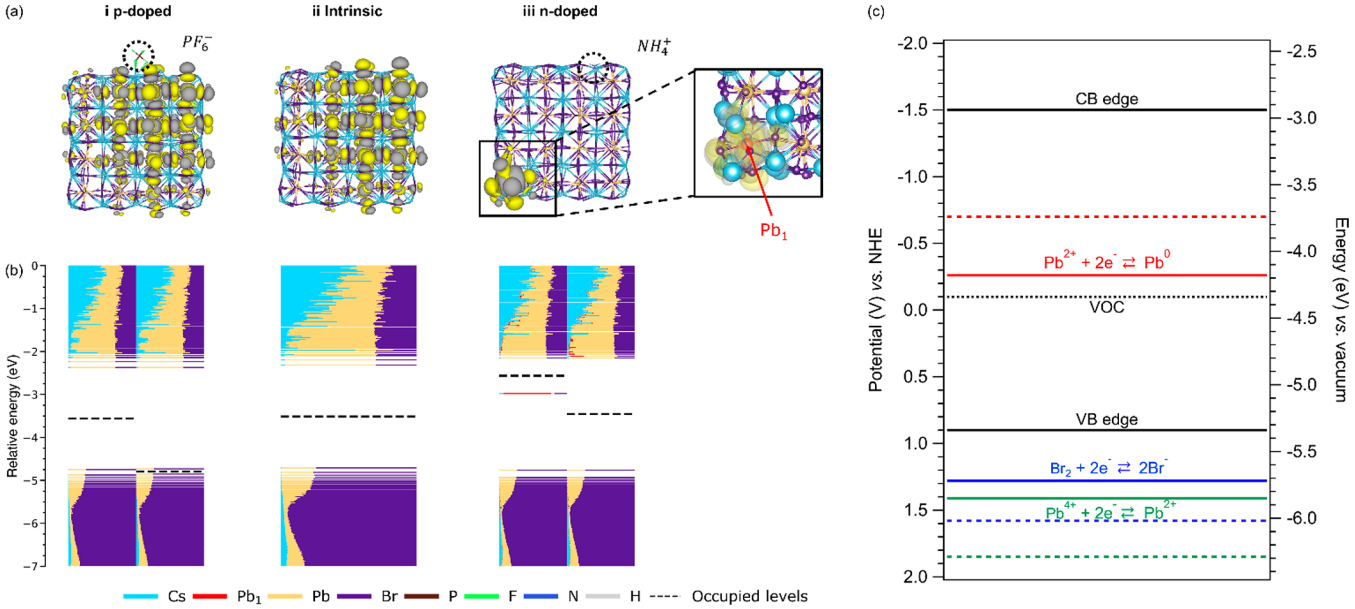

Figure 2. Effect of doping on the electronic structure of a $CsPbBr_3$ NC. (a) Contour plots of the ($\alpha-$) HOMO at 0.005 e^-/bohr^3 for p-doped, n-doped, and intrinsic $CsPbBr_3$ NCs. The p-doped (n-doped) NC has been charged with one hole (electron), compensated by a PF_6^- (NH_4^+) counterion. (b) DOS of each NC, where every line corresponds to a molecular orbital (MO). The relative contributions of specific atoms or elements to each MO are given by the length of the colored line segments. MOs are occupied below the dotted line and empty above it. The doped systems have an odd number of electrons and are computed as spin-unrestricted. The spin-up and spin-down orbitals are plotted separately on the left and right side of the graph, respectively. (c) Energy diagram, indicating the energy level of the VB edge (+0.9 V, as found in the previous section), CB edge (−1.5 V, obtained by adding the optical bandgap to the VB edge position), and V_{OC} (−0.1 V) of the measured $CsPbBr_3$ NCs. Red, blue, and green lines are the formal potentials of various electrochemical half-reactions of Pb^{2+} and Br^- in propylene carbonate. The dashed lines indicate schematically the expected formal potentials of the cathodic and anodic decomposition reactions, shifted by $\frac{RT}{nF}\ln K_{sp}$ compared to the normal lines, where in this example K_{sp} is taken to be 10^{-15} mol^5/L^5.

background currents, either with residual impurities such as water or with ligands or the perovskite material itself (*vide infra*). We therefore turn to spectro-electrochemical measurements to get more insight into the effect of the positive potential on the optical properties of the NCs. As can be seen in Figure 1b, the PL starts to decrease at potentials above +0.7 V, and at +1.2 V the PL is reduced to 84% of its initial value. However, unlike the current in the CV measurement, the PL decrease is reversible, returning to ∼98% of its initial intensity in the reverse scan (inset of Figure 1c). The reversible reduction of the PL intensity *could* indicate hole injection into the VB, as this would give rise to Auger recombination of the positive trions that form after light absorption. However, a change of the PL intensity could also be related to filling of in-gap trap states or the formation of new traps due to electrochemical surface reactions.[50,51] Therefore, reversible PL quenching alone does not prove hole injection, and we turn to changes in the optical absorption and conductivity to further investigate what happens.

Figure 1d shows the differential absorbance of the NC electrode as a function of the applied potential. An increase or decrease of the absorbance, compared to the absorbance at V_{OC}, is marked by red and blue colors, respectively. In Figure 1d, a small bleach of the band edge absorption can be observed for potentials above +0.9 V. As also displayed in Figure 1e, this bleach is reversible and disappears again upon lowering the potential below +0.9 V (see inset), indicating that the feature is not due to the irreversible degradation of the NC electrode. In contrast to the quenching of the PL, a band edge absorption bleach cannot be caused by the formation of trap states, but results from state filling of holes in the VB.

These $CsPbBr_3$ NCs are cubes with an edge length of ∼10 nm. Since the exciton Bohr radius in $CsPbBr_3$ is ∼7 nm,[52−54] this implies that they are only weakly confined.[55,56] For strongly confined quantum dots it is straightforward to derive the density of injected charges from the relative change in absorption. For weakly confined systems the relation is more complex. However, in order to obtain a rough estimate of the injected hole density, we assume that a state-counting method used for quantum-confined systems still holds, so that $\langle h\rangle = g_h \frac{\Delta A}{A_0}$, where $\langle h\rangle$ is the number of holes per NC, g_h the degeneracy of the lowest VB state, ΔA the absorption bleach, and A_0 the steady-state absorption.[57] Using a VB degeneracy of 2,[55,58] and a maximum bleach of $\frac{\Delta A}{A_0} = 0.1$ (see Figure S-8), we estimate a maximum doping density of ∼0.2 h^+/NC, equivalent to a hole density of $\sim 2 \times 10^{17}$ cm^{-3}.

The hallmark of successful electronic doping of semiconductors is an increase in the electronic conductivity. Therefore, we performed electrochemical transistor measurements using a film of perovskite NCs on an interdigitated gold source−drain electrode (see Figure 1f). Details of the measurements are given in SI-5. Figure 1f plots the conductivity of the film as a function of potential in a cyclic fashion and shows a rapid increase in conductivity at +0.9 V. As was the case for the PL and the absorption, the change in conductivity with potential is reversible. The maximum conductivity that we measured was 35 μS/cm at +1.05 V. Together with the hole density of 2×10^{17} cm^{-3} estimated above, this corresponds to a hole mobility of $\sim 1 \times 10^{-3}$ cm^2/(V·s). Both conductivity and mobility values are reasonable for nanocrystal films with relatively long ligands, and similar to

https://doi.org/10.1021/acsenergylett.1c00970
ACS Energy Lett. 2021, 6, 2519−2525

those measured with electrochemical transistor measurements on n-doped CdSe NC films.[59,60]

The combination of the spectro-electrochemical absorption and PL experiments with the electrochemical transistor measurements clearly shows that the hole concentration is varied in a controllable and reversible way, demonstrating successful electrochemical p-doping of the $CsPbBr_3$ NC films. Quantification of the VB position is most easily done by the absorption bleach, as that scales linearly with the hole concentration. For strongly confined systems, when only the HOMO level would be populated, that is relatively straightforward. However, as already stated above, for weakly confined or bulk materials with excitonic absorption, the analysis is more complicated. Therefore, we refrain from a detailed quantification and only remark that the changes in absorption have an onset around +0.9 V vs NHE (= −5.4 V vs vacuum), which should roughly correspond to the VB edge.

In addition to investigating p-doping of $CsPbBr_3$ NCs, we also applied negative potentials to investigate n-doping. In accordance with previous reports by Samu et al.,[46] we observed that injected electrons were lost to Pb^{2+} reduction before the CB edge could be reached (see Figures S-9 and S-10). This caused rapid irreversible loss of the PL, irreversible changes of the absorption, and the formation of a clearly visible metallic Pb^0 layer, as confirmed by XRD and XPS measurements (Figures S-11 and S-12). Hence, for cathodic potentials, it seems impossible to inject electrons into the CB in a reversible way.

To understand the difference between n- and p-doping, we performed DFT calculations on the charging of a $CsPbBr_3$ NC, as summarized in Figure 2. We built a cubic $CsPbBr_3$ NC model, following the approach of Ten Brinck et al.[61] As shown in Figure 2-ii, the intrinsic (i.e., charge balanced) model NC has a clean bandgap and a HOMO that is delocalized over the entire system. Electrochemical injection of one hole into the system is achieved by adding a negative PF_6^- counterion so that the entire system retains charge neutrality.[62] As can be seen in Figure 2a-i, this does not significantly affect the electronic structure of the NC: the HOMO remains delocalized over the NC (Figure 2a-i) and is now singly occupied due to the presence of a hole; no localized states appear in the density of states (DOS) (Figure 2b-i). In contrast, injection of an electron (by adding a NH_4^+ counterion) introduces a singly populated localized state on a single lead ion (Figure 2a-iii) that appears as a localized state in the bandgap (Figure 2b-iii). NH_4^+ was used instead of Bu_4N^+ due to its smaller size and consequently lower computational cost.[62] These results confirm that the addition of electrons immediately results in Pb^{2+} reduction. This is a form of doping compensation that prevents n-doping of the material and will result in cathodic decomposition before the Fermi level moves close enough to the CB to significantly change the electron concentration. On the other hand, the $CsPbBr_3$ NC is much less sensitive to anodic decomposition, allowing the addition of holes via electrochemical doping. This is in line with our experimental observation that p-doping can be performed reversibly, but that n-doping leads to Pb^{2+} reduction and cathodic decomposition.

The fact that p-doping can be achieved does not imply the p-doped NCs are indefinitely stable. Samu et al. investigated halide perovskite thin films under anodic conditions and have not reported reversible p-doping, but rather a sequence of decomposition reactions.[46] When we performed identical experiments on $CsPbBr_3$ NCs synthesized via the method of Protesescu et al.,[49] we did not observe evidence of p-doping (Figure S-13). This suggests that the electrochemical stability of perovskite NCs is subtle and likely dominated by the surface termination. The main difference between the NCs synthesized following Imran et al. and Protesescu et al. is that the former synthesis results in a higher surface density of oleylammonium ligands (due to the bromide-rich synthesis conditions), as evidenced by a much higher colloidal stability upon washing. To illustrate our point, we show an overview of standard reduction potentials of possible decomposition reactions, as well as the CB and VB positions of the $CsPbBr_3$ NCs, in Figure 2c. The most likely candidate reaction for cathodic decomposition is the following:

$$CsPbBr_3 + 2e^- \rightleftarrows Pb^0 + Cs^+ + 3Br^- \quad (1)$$

Indeed, XPS spectra, acquired before and after application of an anodic potential (−1.46 V), show a shift of the Pb 4f XPS peaks to a lower binding energy, in agreement with the decrease of the oxidation state of Pb (Figure S-12).

At the anodic side, we could consider bromide oxidation (reaction 2) or Pb^{2+} oxidation (reaction 3) to cause anodic decomposition:

$$CsPbBr_3 \rightleftarrows Pb^{2+} + Cs^+ + \frac{3}{2}Br_2 + 3e^- \quad (2)$$

$$CsPbBr_3 \rightleftarrows Pb^{4+} + Cs^+ + 3Br^- + 2e^- \quad (3)$$

XPS spectra acquired before and after application of a positive potential show no changes in the Pb 4f peaks and a shift of the Br 3d peaks to higher binding energies (Figure S-12). This suggests that reaction 2 is the more relevant reaction. It also shows that, in spite of the reversible hole injection, some Br^- oxidation does take place. This probably explains the irreversible anodic current observed in the CV measurements (Figure 1a). Most likely Br^- oxidation occurs in parallel to, and in competition with, hole injection into the VB.

The standard reduction potentials of reactions 1−3 are related to the standard reduction potential of the free ions—$Pb^{2+} + 2e^- \rightarrow Pb^0$; $Br_2 + 2e^- \rightarrow 2Br^-$; and $Pb^{4+} + 2e^- \rightarrow Pb^{2+}$, respectively—although they are stabilized compared to those free ion reactions due to binding to the other ions in the perovskite crystal lattice. We estimated the standard reduction potentials of these latter reactions in propylene carbonate via CV (see SI-14). The obtained values are similar, albeit somewhat shifted, to those reported for the same reactions in water,[63] and are marked as red, blue, and green horizontal solid lines in Figure 2c, respectively.

As derived in SI-15, the formal reduction potential of reaction 1 is shifted by $\frac{RT}{nF}\ln K_{sp}$ compared to the formal reduction potential of $Pb^{2+} + 2e^- \rightarrow Pb^0$. Here $K_{sp} = [Cs^+][Pb^{2+}][Br^-]^3$ is the solubility product of $CsPbBr_3$ in the same solvent and n is the number of electrons involved in the reaction. Similarly, the formal potentials of reactions 2 and 3 are shifted by $-\frac{RT}{nF}\ln K_{sp}$ compared to the free ion reactions, with $n = 3$ for (2) and $n = 2$ for (3) (see SI-15).

This indicates that, in solvents wherein $CsPbBr_3$ is poorly soluble and K_{sp} is smaller than 1, the cathodic dissolution will occur at more negative potentials than the reduction of free Pb^{2+} ions, and the anodic dissolution will occur at more positive potentials than the oxidation of free Br^- and free Pb^{2+}. For instance, the reported value of K_{sp} for $CsPbBr_3$ in a

https://doi.org/10.1021/acsenergylett.1c00970
ACS Energy Lett. 2021, 6, 2519−2525

mixture of γ-butyrolactone (GBL) and dimethyl sulfoxide (DMSO) is $\sim 10^{-3}$ mol^5/L^5, corresponding to a stabilization of $\sim 177/n$ mV.[64] Propylene carbonate, the solvent used in the electrochemical experiments in the current paper, was chosen because the $CsPbBr_3$ NC films do not readily dissolve in it (unlike in, e.g., DMSO), and hence the expected solubility product is much lower, and the expected stabilization greater, than in GBL/DMSO. Unfortunately, quantitative information on the solubility of $CsPbBr_3$ in propylene carbonate is, to the best of our knowledge, not available. The dashed lines in Figure 2c indicate schematically where the formal potential of the decomposition reactions 1−3 could lie, in this example for $K_{sp} = 10^{-15}$ mol^5/L^5.

Figure 2c shows that the cathodic decomposition potential of $CsPbBr_3$ lies well positive of the CB potential (unless $\frac{RT}{2F}\ln K_{sp} < -1.25$ V, i.e., $K_{sp} < 5 \times 10^{-43}$ mol^5/L^5, which seems unrealistic). This implies that the cathodic decomposition reaction will occur before electron injection into the CB, resulting in n-doping compensation through Pb^0 formation. At the anodic side, Br^- oxidation would be expected to occur well before Pb^{2+} oxidation. However, in both cases we estimate the formal potentials of the anodic decomposition to lie at more positive potentials than the VB of $CsPbBr_3$. It is interesting to note that the situation will be very different for Sn^{2+}-based perovskites. As the standard reduction potential of Sn^{4+}/Sn^{2+} in propylene carbonate lies at 0.11 V vs NHE (see SI-14), oxidation of Sn^{2+} is expected to take place before Br^- oxidation and most likely before the VB is reached, making p-doping very difficult for these systems. In double perovskites, like, e.g., $Cs_2AgBiBr_6$, the reduction of Ag^+ ($E^{0\prime}$ = 0.8 V vs NHE in water)[63] and Bi^{3+} ($E^{0\prime}$ = 0.3 V vs NHE in water)[63] will most likely prevent n-doping, while Br^- oxidation will be the limiting factor for p-doping.

The above discussion pertains to bulk $CsPbBr_3$. The initial electrochemical reactions on the surface of $CsPbBr_3$ NCs will occur at sites that are under-coordinated compared to the bulk, and hence the formal potentials of these will be less negative for surface reduction and less positive for surface oxidation, compared to the bulk formal potentials, and will likely lie between the solid and dashed lines in Figure 2c. Moreover, the formal potentials are also sensitive to bonds formed between ligands and surface ions.

From our measurements and the preceding discussion, it is likely that, upon moving the Fermi level to positive potentials, the VB of $CsPbBr_3$ NCs is reached before the formal potential of the anodic decomposition reactions. However, the difference in potential may be small. This suggests that the stability of p-doped $CsPbBr_3$ NCs will be sensitive to changes in surface Br^- coordination (shifting the formal potential of reaction 2) and the solvent (affecting K_{sp}) as well as the exact position of the VB, which is known to be affected by the surface passivation.[65,66] In addition, if Br^- oxidation via reaction 2 is irreversible, the stability of p-doped $CsPbBr_3$ will be limited, since the oxidation rate will not be zero when the Fermi level is in, or near, the VB. This is in line with our observations that, over time scales of minutes, the PL of p-doped $CsPbBr_3$ decreases irreversibly and with the XPS results that show that some Br^- oxidation does take place at cathodic potentials. Increasing the stability of p-doped $CsPbBr_3$ NCs thus requires improved surface passivation strategies, with strongly binding surfactants, to further reduce the rate of surface oxidation.

To summarize, we report reversible electrochemical p-doping of $CsPbBr_3$ NCs. We demonstrate that raising the applied potential above +0.9 V vs NHE simultaneously quenches the PL, bleaches the band edge absorption, and significantly increases the conductivity, all consistent with charge injection in the VB edge. By combining experimental results with DFT calculations, we conclude that p-doping of $CsPbBr_3$ NC electrodes is possible, although their stability is limited due to Br^- oxidation. Increasing this stability further will require optimized surface passivation strategies. In contrast, n-doping is impossible due to facile Pb^{2+} reduction.

■ ASSOCIATED CONTENT

Supporting Information

The Supporting Information is available free of charge at https://pubs.acs.org/doi/10.1021/acsenergylett.1c00970.

Experimental methods, optical spectra and TEM of NC solution and electrode, new electrodes, reproducibility of PL measurements, conductance measurements, film thickness, conductivity and mobility calculations, spectroscopic data n-doping, used electrodes, lead film XRD, XPS analysis of measured films, spectro-electrochemical measurements and films of $CsPbBr_3$ by different synthesis method, CV determination of formal potentials of Pb^{2+} reduction and oxidation, Br^- oxidation and Sn^{2+} reduction and oxidation, and thermodynamic discussion of cathodic and anodic decomposition reactions (PDF)

■ AUTHOR INFORMATION

Corresponding Author

Arjan J. Houtepen − *Optoelectronic Materials Section, Faculty of Applied Sciences, Delft University of Technology, 2629HZ Delft, The Netherlands;* orcid.org/0000-0001-8328-443X; Email: a.j.houtepen@tudelft.nl

Authors

Jence T. Mulder − *Optoelectronic Materials Section, Faculty of Applied Sciences, Delft University of Technology, 2629HZ Delft, The Netherlands;* orcid.org/0000-0002-4397-1347

Indy du Fossé − *Optoelectronic Materials Section, Faculty of Applied Sciences, Delft University of Technology, 2629HZ Delft, The Netherlands;* orcid.org/0000-0002-6808-4664

Maryam Alimoradi Jazi − *Optoelectronic Materials Section, Faculty of Applied Sciences, Delft University of Technology, 2629HZ Delft, The Netherlands*

Liberato Manna − *Optoelectronic Materials Section, Faculty of Applied Sciences, Delft University of Technology, 2629HZ Delft, The Netherlands; Department of Nanochemistry, Istituto Italiano di Tecnologia (IIT), 16163 Genova, Italy;* orcid.org/0000-0003-4386-7985

Complete contact information is available at: https://pubs.acs.org/10.1021/acsenergylett.1c00970

Notes

The authors declare no competing financial interest.

■ ACKNOWLEDGMENTS

This project has received funding from the European Union's Horizon 2020 research and innovation program under grant agreements no. 766900 (Testing the Large-Scale Limit of Quantum Mechanics), no. 678004 (Doping on Demand), and no. 841109 (Designing Devices by Doping on Demand). This

work was sponsored by NWO Exact and Natural Sciences for the use of supercomputer facilities and was carried out on the Dutch national e-infrastructure with the support of the SURF Cooperative. The authors thank Wiel Evers and John Suijkerbuijk for their help in maintaining and improving the spectro-electrochemical setup. The authors furthermore thank Bart Boshuizen for the help with performing and analyzing the XPS measurements.

REFERENCES

(1) Schmidt, L. C.; Pertegas, A.; Gonzalez-Carrero, S.; Malinkiewicz, O.; Agouram, S.; Minguez Espallargas, G.; Bolink, H. J.; Galian, R. E.; Perez-Prieto, J. Non-Template Synthesis of $CH_3NH_3PbBr_3$ Perovskite Nanoparticles. *J. Am. Chem. Soc.* **2014**, *136*, 850−853.

(2) Adhikari, G. C.; Zhu, H.; Vargas, P. A.; Zhu, P. UV-Green Emission from Organolead Bromide Perovskite Nanocrystals. *J. Phys. Chem. C* **2018**, *122* (26), 15041−15046.

(3) Srivastava, A. K.; Zhang, W.; Schneider, J.; Halpert, J. E.; Rogach, A. L. Luminescent Down-Conversion Semiconductor Quantum Dots and Aligned Quantum Rods for Liquid Crystal Displays. *Adv. Sci.* **2019**, *6* (22), 1901345.

(4) Zou, T.; Liu, X.; Qiu, R.; Wang, Y.; Huang, S.; Liu, C.; Dai, Q.; Zhou, H. Enhanced UV-C Detection of Perovskite Photodetector Arrays via Inorganic $CsPbBr_3$ Quantum Dot Down-Conversion Layer. *Adv. Opt. Mater.* **2019**, *7* (11), 1801812.

(5) Yuan, J.; Hazarika, A.; Zhao, Q.; Ling, X.; Moot, T.; Ma, W.; Luther, J. M. Metal Halide Perovskites in Quantum Dot Solar Cells: Progress and Prospects. *Joule* **2020**, *4* (6), 1160−1185.

(6) Zhou, F.; Li, Z.; Chen, H.; Wang, Q.; Ding, L.; Jin, Z. Application of Perovskite Nanocrystals (NCs)/Quantum Dots (QDs) in Solar Cells. *Nano Energy* **2020**, *73*, 104757.

(7) Kim, Y.-C.; Jeong, H.-J.; Kim, S.-T.; Song, Y. H.; Kim, B. Y.; Kim, J. P.; Kang, B. K.; Yun, J.-H.; Jang, J.-H. Luminescent Down-Shifting $CsPbBr_3$ Perovskite Nanocrystals for Flexible $Cu(In,Ga)Se_2$ Solar Cells. *Nanoscale* **2020**, *12* (2), 558−562.

(8) Palazon, F.; Di Stasio, F.; Akkerman, Q. A.; Krahne, R.; Prato, M.; Manna, L. Polymer-Free Films of Inorganic Halide Perovskite Nanocrystals as UV-to-White Color-Conversion Layers in LEDs. *Chem. Mater.* **2016**, *28* (9), 2902−2906.

(9) Yan, F.; Tan, S. T.; Li, X.; Demir, H. V. Light Generation in Lead Halide Perovskite Nanocrystals: LEDs, Color Converters, Lasers, and Other Applications. *Small* **2019**, *15* (47), 1902079.

(10) Hassan, Y.; Park, J. H.; Crawford, M. L.; Sadhanala, A.; Lee, J.; Sadighian, J. C.; Mosconi, E.; Shivanna, R.; Radicchi, E.; Jeong, M.; Yang, C.; Choi, H.; Park, S. H.; Song, M. H.; De Angelis, F.; Wong, C. Y.; Friend, R. H.; Lee, B. R.; Snaith, H. J. Ligand-Engineered Bandgap Stability in Mixed-Halide Perovskite LEDs. *Nature* **2021**, *591* (7848), 72−77.

(11) Kovalenko, M. V.; Protesescu, L.; Bodnarchuk, M. I. Properties and Potential Optoelectronic Applications of Lead Halide Perovskite Nanocrystals. *Science* **2017**, *358* (6364), 745−750.

(12) Zhang, C.; Wang, S.; Li, X.; Yuan, M.; Turyanska, L.; Yang, X. Core/Shell Perovskite Nanocrystals: Synthesis of Highly Efficient and Environmentally Stable $FAPbBr_3/CsPbBr_3$ for LED Applications. *Adv. Funct. Mater.* **2020**, *30* (31), 1910582.

(13) Stranks, S. D.; Snaith, H. J. Metal-Halide Perovskites for Photovoltaic and Light-Emitting Devices. *Nat. Nanotechnol.* **2015**, *10* (5), 391−402.

(14) Zhao, B.; Bai, S.; Kim, V.; Lamboll, R.; Shivanna, R.; Auras, F.; Richter, J. M.; Yang, L.; Dai, L.; Alsari, M.; She, X. J.; Liang, L.; Zhang, J.; Lilliu, S.; Gao, P.; Snaith, H. J.; Wang, J.; Greenham, N. C.; Friend, R. H.; Di, D. High-Efficiency Perovskite−polymer Bulk Heterostructure Light-Emitting Diodes. *Nat. Photonics* **2018**, *12* (12), 783−789.

(15) Xu, B.; Wang, W.; Zhang, X.; Cao, W.; Wu, D.; Liu, S.; Dai, H.; Chen, S.; Wang, K.; Sun, X. Bright and Efficient Light-Emitting Diodes Based on MA/Cs Double Cation Perovskite Nanocrystals. *J. Mater. Chem. C* **2017**, *5* (25), 6123−6128.

(16) Lou, S.; Xuan, T.; Liang, Q.; Huang, J.; Cao, L.; Yu, C.; Cao, M.; Xia, C.; Wang, J.; Zhang, D.; Li, H. Controllable and Facile Synthesis of $CsPbBr_3$-Cs_4PbBr_6 Perovskite Composites in Pure Polar Solvent. *J. Colloid Interface Sci.* **2019**, *537*, 384−388.

(17) Hassan, Y.; Ashton, O. J.; Park, J. H.; Li, G.; Sakai, N.; Wenger, B.; Haghighirad, A. A.; Noel, N. K.; Song, M. H.; Lee, B. R.; Friend, R. H.; Snaith, H. J. Facile Synthesis of Stable and Highly Luminescent Methylammonium Lead Halide Nanocrystals for Efficient Light Emitting Devices. *J. Am. Chem. Soc.* **2019**, *141* (3), 1269−1279.

(18) Wang, C.; Wang, Z.; Song, Y.; Zhang, X.; Wang, J.; Liu, P.; Cao, H.; Xu, B.; Zhao, M.; Miao, Y.; Guo, J. Facile Synthesis of Perovskite Phosphors and Nanocrystals Using Laundry Detergent by Ultra-Rapid Freezing for Light-Emitting Diodes Application. *J. Lumin.* **2021**, *233*, 117902.

(19) Shamsi, J.; Urban, A. S.; Imran, M.; De Trizio, L.; Manna, L. Metal Halide Perovskite Nanocrystals: Synthesis, Post-Synthesis Modifications, and Their Optical Properties. *Chem. Rev.* **2019**, *119* (5), 3296−3348.

(20) Mandal, S.; Ghosh, S.; Mukherjee, S.; De, C. K.; Roy, D.; Samanta, T.; Mandal, P. K. Unravelling Halide-Dependent Charge Carrier Dynamics in $CsPb(Br/Cl)_3$ Perovskite Nanocrystals. *Nanoscale* **2021**, *13*, 3654−3661.

(21) Giovanni, D.; Righetto, M.; Zhang, Q.; Lim, J. W. M.; Ramesh, S.; Sum, T. C. Origins of the Long-Range Exciton Diffusion in Perovskite Nanocrystal Films: Photon Recycling vs Exciton Hopping. *Light: Sci. Appl.* **2021**, *10* (1), 2.

(22) Kim, S. H.; Park, K.-D.; Lee, H. S. Growth Kinetics and Optical Properties of $CsPbBr_3$ Perovskite Nanocrystals. *Energies* **2021**, *14* (2), 275.

(23) Wang, S.; Yousefi Amin, A. A.; Wu, L.; Cao, M.; Zhang, Q.; Ameri, T. Perovskite Nanocrystals: Synthesis, Stability, and Optoelectronic Applications. *Small Struct.* **2021**, *2* (3), 2000124.

(24) Huang, H.; Bodnarchuk, M. I.; Kershaw, S. V.; Kovalenko, M. V.; Rogach, A. L. Lead Halide Perovskite Nanocrystals in the Research Spotlight: Stability and Defect Tolerance. *ACS Energy Lett.* **2017**, *2* (9), 2071−2083.

(25) Lu, C. H.; Biesold-Mcgee, G. V.; Liu, Y.; Kang, Z.; Lin, Z. Doping and Ion Substitution in Colloidal Metal Halide Perovskite Nanocrystals. *Chem. Soc. Rev.* **2020**, *49* (14), 4953−5007.

(26) Xu, L.; Yuan, S.; Zeng, H.; Song, J. A Comprehensive Review of Doping in Perovskite Nanocrystals/Quantum Dots: Evolution of Structure, Electronics, Optics, and Light-Emitting Diodes. *Mater. Today Nano* **2019**, *6*, 100036.

(27) Cai, W.; Chen, Z.; Chen, D.; Su, S.; Xu, Q.; Yip, H. L.; Cao, Y. High-Performance and Stable $CsPbBr_3$ Light-Emitting Diodes Based on Polymer Additive Treatment. *RSC Adv.* **2019**, *9* (47), 27684−27691.

(28) Du, X.; Wu, G.; Cheng, J.; Dang, H.; Ma, K.; Zhang, Y. W.; Tan, P. F.; Chen, S. High-Quality $CsPbBr_3$ Perovskite Nanocrystals for Quantum Dot Light-Emitting Diodes. *RSC Adv.* **2017**, *7* (17), 10391−10396.

(29) Li, L.; Zheng, W.; Wan, Q.; Liu, M.; Zhang, Q.; Zhang, C.; Yan, R.; Feng, X.; Kong, L. $CsPbBr_3$ Nanocrystal Light-Emitting Diodes with Efficiency up to 13.4% Achieved by Careful Surface Engineering and Device Engineering. *J. Phys. Chem. C* **2021**, *125* (5), 3110−3118.

(30) Geuchies, J. J.; Brynjarsson, B.; Grimaldi, G.; Gudjonsdottir, S.; Van Der Stam, W.; Evers, W. H.; Houtepen, A. J. Quantitative Electrochemical Control over Optical Gain in Quantum-Dot Solids. *ACS Nano* **2021**, *15* (1), 377−386.

(31) Gerischer, H. On the Stability of Semiconductor Electrodes Against Photodecomposition. *J. Electroanal. Chem. Interfacial Electrochem.* **1977**, *82* (1−2), 133−143.

(32) Tsur, Y.; Riess, I. Self-Compensation in Semiconductors. *Phys. Rev. B: Condens. Matter Mater. Phys.* **1999**, *60* (11), 8138−8146.

(33) Phung, N.; Félix, R.; Meggiolaro, D.; Al-Ashouri, A.; Sousa E Silva, G.; Hartmann, C.; Hidalgo, J.; Köbler, H.; Mosconi, E.; Lai, B.; Gunder, R.; Li, M.; Wang, K. L.; Wang, Z. K.; Nie, K.; Handick, E.; Wilks, R. G.; Marquez, J. A.; Rech, B.; Unold, T.; Correa-Baena, J. P.; Albrecht, S.; De Angelis, F.; Bär, M.; Abate, A. The Doping

https://doi.org/10.1021/acsenergylett.1c00970
ACS Energy Lett. 2021, 6, 2519−2525

Mechanism of Halide Perovskite Unveiled by Alkaline Earth Metals. *J. Am. Chem. Soc.* **2020**, *142* (5), 2364−2374.
(34) Zhou, S.; Ma, Y.; Zhou, G.; Xu, X.; Qin, M.; Li, Y.; Hsu, Y. J.; Hu, H.; Li, G.; Zhao, N.; Xu, J.; Lu, X. Ag-Doped Halide Perovskite Nanocrystals for Tunable Band Structure and Efficient Charge Transport. *ACS Energy Lett.* **2019**, *4* (2), 534−541.
(35) Gaulding, E. A.; Hao, J.; Kang, H. S.; Miller, E. M.; Habisreutinger, S. N.; Zhao, Q.; Hazarika, A.; Sercel, P. C.; Luther, J. M.; Blackburn, J. L. Conductivity Tuning via Doping with Electron Donating and Withdrawing Molecules in Perovskite $CsPbI_3$ Nanocrystal Films. *Adv. Mater.* **2019**, *31* (27), 1902250.
(36) Amerling, E.; Lu, H.; Larson, B. W.; Maughan, A. E.; Phillips, A.; Lafalce, E.; Whittaker-Brooks, L.; Berry, J. J.; Beard, M. C.; Vardeny, Z. V.; Blackburn, J. L. A Multi-Dimensional Perspective on Electronic Doping in Metal Halide Perovskites. *ACS Energy Lett.* **2021**, *6* (3), 1104−1123.
(37) Amelia, M.; Lincheneau, C.; Silvi, S.; Credi, A. Electrochemical Properties of CdSe and CdTe Quantum Dots. *Chem. Soc. Rev.* **2012**, *41* (17), 5728−5743.
(38) Haram, S. K.; Quinn, B. M.; Bard, A. J. Electrochemistry of CdS Nanoparticles: A Correlation between Optical and Electrochemical Band Gaps. *J. Am. Chem. Soc.* **2001**, *123* (36), 8860−8861.
(39) Boehme, S. C.; Walvis, T. A.; Infante, I.; Grozema, F. C.; Vanmaekelbergh, D.; Siebbeles, L. D. A.; Houtepen, A. J. Electrochemical Control over Photoinduced Electron Transfer and Trapping in CdSe-CdTe Quantum-Dot Solids. *ACS Nano* **2014**, *8* (7), 7067−7077.
(40) van der Stam, W.; Gudjonsdottir, S.; Evers, W. H.; Houtepen, A. J. Switching between Plasmonic and Fluorescent Copper Sulfide Nanocrystals. *J. Am. Chem. Soc.* **2017**, *139* (37), 13208−13217.
(41) Gudjonsdottir, S.; Van Der Stam, W.; Koopman, C.; Kwakkenbos, B.; Evers, W. H.; Houtepen, A. J. On the Stability of Permanent Electrochemical Doping of Quantum Dot, Fullerene, and Conductive Polymer Films in Frozen Electrolytes for Use in Semiconductor Devices. *ACS Appl. Nano Mater.* **2019**, *2* (8), 4900−4909.
(42) Tajik, S.; Beitollahi, H.; Nejad, F. G.; Shoaie, I. S.; Khalilzadeh, M. A.; Asl, M. S.; Van Le, Q.; Zhang, K.; Jang, H. W.; Shokouhimehr, M. Recent Developments in Conducting Polymers: Applications for Electrochemistry. *RSC Adv.* **2020**, *10* (62), 37834−37856.
(43) Neusser, D.; Malacrida, C.; Kern, M.; Gross, Y. M.; van Slageren, J.; Ludwigs, S. High Conductivities of Disordered P_3HT Films by an Electrochemical Doping Strategy. *Chem. Mater.* **2020**, *32* (14), 6003−6013.
(44) Pumera, M.; Sofer, Z.; Ambrosi, A. Layered Transition Metal Dichalcogenides for Electrochemical Energy Generation and Storage. *J. Mater. Chem. A* **2014**, *2* (24), 8981−8987.
(45) Chia, X.; Eng, A. Y. S.; Ambrosi, A.; Tan, S. M.; Pumera, M. Electrochemistry of Nanostructured Layered Transition-Metal Dichalcogenides. *Chem. Rev.* **2015**, *115* (21), 11941−11966.
(46) Samu, G. F.; Scheidt, R. A.; Kamat, P. V.; Janáky, C. Electrochemistry and Spectroelectrochemistry of Lead Halide Perovskite Films: Materials Science Aspects and Boundary Conditions. *Chem. Mater.* **2018**, *30* (3), 561−569.
(47) Lorenzon, M.; Sortino, L.; Akkerman, Q.; Accornero, S.; Pedrini, J.; Prato, M.; Pinchetti, V.; Meinardi, F.; Manna, L.; Brovelli, S. Role of Nonradiative Defects and Environmental Oxygen on Exciton Recombination Processes in $CsPbBr_3$ Perovskite Nanocrystals. *Nano Lett.* **2017**, *17* (6), 3844−3853.
(48) Imran, M.; Caligiuri, V.; Wang, M.; Goldoni, L.; Prato, M.; Krahne, R.; De Trizio, L.; Manna, L. Benzoyl Halides as Alternative Precursors for the Colloidal Synthesis of Lead-Based Halide Perovskite Nanocrystals. *J. Am. Chem. Soc.* **2018**, *140* (7), 2656−2664.
(49) Protesescu, L.; Yakunin, S.; Bodnarchuk, M. I.; Krieg, F.; Caputo, R.; Hendon, C. H.; Yang, R. X.; Walsh, A.; Kovalenko, M. V. Nanocrystals of Cesium Lead Halide Perovskites ($CsPbX_3$, X = Cl, Br, and I): Novel Optoelectronic Materials Showing Bright Emission with Wide Color Gamut. *Nano Lett.* **2015**, *15* (6), 3692−3696.
(50) Grimaldi, G.; Geuchies, J. J.; van der Stam, W.; du Fossé, I.; Brynjarsson, B.; Kirkwood, N.; Kinge, S.; Siebbeles, L. D. A.; Houtepen, A. J. Spectroscopic Evidence for the Contribution of Holes to the Bleach of Cd-Chalcogenide Quantum Dots. *Nano Lett.* **2019**, *19* (5), 3002−3010.
(51) Boehme, S. C.; Azpiroz, J. M.; Aulin, Y. V.; Grozema, F. C.; Vanmaekelbergh, D.; Siebbeles, L. D. A.; Infante, I.; Houtepen, A. J. Density of Trap States and Auger-Mediated Electron Trapping in CdTe Quantum-Dot Solids. *Nano Lett.* **2015**, *15* (5), 3056−3066.
(52) Yang, H.; Feng, Y.; Tu, Z.; Su, K.; Fan, X.; Liu, B.; Shi, Z.; Zhang, Y.; Zhao, C.; Zhang, B. Blue Emitting $CsPbBr_3$ Perovskite Quantum Dot Inks Obtained from Sustained Release Tablets. *Nano Res.* **2019**, *12* (12), 3129−3134.
(53) Ha, S. T.; Su, R.; Xing, J.; Zhang, Q.; Xiong, Q. Metal Halide Perovskite Nanomaterials: Synthesis and Applications. *Chem. Sci.* **2017**, *8* (4), 2522−2536.
(54) Worku, M.; Tian, Y.; Zhou, C.; Lin, H.; Chaaban, M.; Xu, L.; He, Q.; Beery, D.; Zhou, Y.; Lin, X.; Su, Y.; Xin, Y.; Ma, B. Hollow Metal Halide Perovskite Nanocrystals with Efficient Blue Emissions. *Sci. Adv.* **2020**, *6* (17), eaaz5961.
(55) Butkus, J.; Vashishtha, P.; Chen, K.; Gallaher, J. K.; Prasad, S. K. K.; Metin, D. Z.; Laufersky, G.; Gaston, N.; Halpert, J. E.; Hodgkiss, J. M. The Evolution of Quantum Confinement in $CsPbBr_3$ Perovskite Nanocrystals. *Chem. Mater.* **2017**, *29* (8), 3644−3652.
(56) Geiregat, P.; Maes, J.; Chen, K.; Drijvers, E.; De Roo, J.; Hodgkiss, J. M.; Hens, Z. Using Bulk-like Nanocrystals to Probe Intrinsic Optical Gain Characteristics of Inorganic Lead Halide Perovskites. *ACS Nano* **2018**, *12*, 10178−10188.
(57) Boehme, S. C.; Azpiroz, J. M.; Aulin, Y. V.; Grozema, F. C.; Vanmaekelbergh, D.; Siebbeles, L. D. A.; Infante, I.; Houtepen, A. J. Density of Trap States and Auger-Mediated Electron Trapping in CdTe Quantum-Dot Solids. *Nano Lett.* **2015**, *15* (5), 3056−3066.
(58) Makarov, N. S.; Guo, S.; Isaienko, O.; Liu, W.; Robel, I.; Klimov, V. I. Spectral and Dynamical Properties of Single Excitons, Biexcitons, and Trions in Cesium-Lead-Halide Perovskite Quantum Dots. *Nano Lett.* **2016**, *16* (4), 2349−2362.
(59) Yu, D.; Wehrenberg, B. L.; Jha, P.; Ma, J.; Guyot-Sionnest, P. Electronic Transport of N-Type CdSe Quantum Dot Films: Effect of Film Treatment. *J. Appl. Phys.* **2006**, *99* (10), 104315.
(60) Yu, D. N-Type Conducting CdSe Nanocrystal Solids. *Science* **2003**, *300* (5623), 1277−1280.
(61) Ten Brinck, S.; Zaccaria, F.; Infante, I. Defects in Lead Halide Perovskite Nanocrystals: Analogies and (Many) Differences with the Bulk. *ACS Energy Lett.* **2019**, *4* (11), 2739−2747.
(62) Du Fossé, I.; Ten Brinck, S.; Infante, I.; Houtepen, A. J. Role of Surface Reduction in the Formation of Traps in N-Doped II-VI Semiconductor Nanocrystals: How to Charge without Reducing the Surface. *Chem. Mater.* **2019**, *31* (12), 4575−4583.
(63) Haynes, W. M.; Lide, D. R.; Bruno, T. J. *CRC Handbook of Chemistry and Physics*, 97th ed.; CRC Press: Boca Raton, FL, 2016.
(64) Fan, Y.; Fang, J.; Chang, X.; Tang, M. C.; Barrit, D.; Xu, Z.; Jiang, Z.; Wen, J.; Zhao, H.; Niu, T.; Smilgies, D. M.; Jin, S.; Liu, Z.; Li, E. Q.; Amassian, A.; Liu, S.; Zhao, K. Scalable Ambient Fabrication of High-Performance $CsPbI_2Br$ Solar Cells. *Joule* **2019**, *3* (10), 2485−2502.
(65) Kroupa, D. M.; Vörös, M.; Brawand, N. P.; McNichols, B. W.; Miller, E. M.; Gu, J.; Nozik, A. J.; Sellinger, A.; Galli, G.; Beard, M. C. Tuning Colloidal Quantum Dot Band Edge Positions through Solution-Phase Surface Chemistry Modification. *Nat. Commun.* **2017**, *8* (1), 15257.
(66) Brown, P. R.; Kim, D.; Lunt, R. R.; Zhao, N.; Bawendi, M. G.; Grossman, J. C.; Bulović, V. Energy Level Modification in Lead Sulfide Quantum Dot Thin Films through Ligand Exchange. *ACS Nano* **2014**, *8*, 5863−5872.

https://doi.org/10.1021/acsenergylett.1c00970
ACS Energy Lett. 2021, 6, 2519−2525